



## Effect of milling time on the microstructure of Al<sub>2</sub>O<sub>3</sub>-Mo Nanocomposite

A. Mortazavi, M. Razavi\*, T. Ebadzadeh, A. Sedaghat Ahangari Hossein Zadeh

Department of Ceramic, Materials and Energy Research Center, Karaj, Iran

### PAPER INFO

#### Paper history:

Received 07 November 2015

Accepted in revised form 14 February 2016

#### Keywords:

Nanocomposite  
Molybdenum  
SPS

### ABSTRACT

In this paper, the effect of milling time in the production of Al<sub>2</sub>O<sub>3</sub>-Mo nanocomposites via mechanical milling is investigated. The crystallite size of Al<sub>2</sub>O<sub>3</sub>- 20 vol.% Mo powder mixtures grinded using a planetary ball mill are determined at different milling times using the XRD technique. The crystallite sizes of the milled powders are confirmed to be in nano-meter scale. The results show that increasing the milling time leads to a decrease in the crystallite size as well as in the unit cell volume. Furthermore, microstructural investigations using SEM imaging show uniform distribution of ultrafine second phase in the matrix. It is shown that the Al<sub>2</sub>O<sub>3</sub>-Mo nanocomposite is produced successfully after five hours of milling time.

## 1. INTRODUCTION

Mechanical milling is a high-energy ball milling process in which, constituent powders are repeatedly deformed, fractured and welded by grinding media to form a homogeneous alloyed microstructure or uniformly dispersed particulates in a matrix [1-4]. Fracture and welding are known to be two major mechanisms affecting the structural evolution during the mechanical milling. The process needs at least one fairly ductile metal to act as host or binder. The main purposes of the milling process are to decrease the particle sizes (breaking down the material), mixing, blending and particle shaping. These competing events of cold welding (with plastic deformation and agglomeration) and fracturing (size reduction) continues repeatedly during the milling period. This process could successfully produce fine and uniform dispersions of oxide particles in contrast with more conventional powder metallurgy methods. This advantage has made the mechanical milling technique suitable for fabrication of ceramic-metal composites [1, 18] and other nanostructured materials [10, 11, 17 and 19].

Ceramic-metal composites have gained considerable attention due to their increased fracture toughness when compared to traditional ceramics. For example, Al<sub>2</sub>O<sub>3</sub>-based ceramic matrix composites (CMCs) continue to find a wide range of possible advanced applications

provided that an optimum combination of high strength and ductility is achieved for these composites. The Al<sub>2</sub>O<sub>3</sub> has been previously studied in ceramic/ceramic nanocomposite systems such as Al<sub>2</sub>O<sub>3</sub>/SiC [5, 6]. Copper, Nickel, Chromium and Tungsten are mostly used for improving the properties of alumina ceramics [7, 8]. However, in the past two decades, Molybdenum-Alumina composites have been also investigated due to the interesting properties of Molybdenum particles as matrix modifiers. Particularly, slightly lower coefficient of thermal expansion with respect to the Al<sub>2</sub>O<sub>3</sub> matrix along with the high melting temperature of Molybdenum make it suitable for high temperature applications [5, 7]. However, it has been found that the size of these metal particles [9] has a profound influence on the toughening effect, these results indicated that coarse Mo particles improved the bridging effect and also the interface of small Mo particles (less than 5 μm) is easily fractured upon crack interaction which decreases the maximum toughness attained and as a consequence, a lower toughness value was achieved.

In this paper, the effect of milling time on the preparation, lattice parameters and morphology of Al<sub>2</sub>O<sub>3</sub>/molybdenum mixed powders via mechanical milling is investigated.

## 2. EXPERIMENTAL PROCEDURES

Commercial purity Al<sub>2</sub>O<sub>3</sub> powder (Merck, Art. No: 1056, d<sub>50</sub>: 80-100 μm) and Molybdenum powder (Martinswerk, d<sub>50</sub>: 5-10 μm) were used as the raw

\*Corresponding Author's Email: [m-razvi@merc.ac.ir](mailto:m-razvi@merc.ac.ir) (M. Razavi)

materials. A 60g mixture of  $\text{Al}_2\text{O}_3$ -20vol. % Mo was milled in a 500 mL stainless steel mixing planetary ball mill for duration of up to 15 hours in argon gas atmosphere. Sampling was performed at different times in order to characterize the milled powders at various periods of time. The ball to powder ratio was 10:1 and the milling speed was preserved at 300 revolutions per minute (rpm).

X-ray diffraction (XRD) analysis was used in order to detect and characterize the phases via a Philips PW3710 model (Cu  $K\alpha$ ) with voltage and current of 30 kV and 25 mA, respectively. Using the diffraction patterns, the crystallite size and lattice strain variations through milling stages were calculated by the Williamson-Hall method for at least three peaks from Equation (1):

$$B\cos\theta = 0.9\lambda/D + 2\eta \sin\theta \quad (1)$$

Where  $B$ ,  $\lambda$ ,  $\theta$ ,  $D$ , and  $\eta$  denote the full width at half maximum (FWHM), wave length, peak position, crystallite size and lattice strain, respectively. The average crystallite size and the lattice strain were then estimated using linear regression on “ $B\cos\theta$ ” vs. “ $2\sin\theta$ ” plotted data.

The lattice constant,  $a_{\text{exp}}$ , was calculated for the cubic system, Equation (2), while using the Bragg equation, Equation (3), to calculate the d-spacing:

$$a_{\text{exp}} = d_{hkl} \sqrt{h^2 + k^2 + l^2} \quad (2)$$

$$d_{hkl} = \frac{\lambda}{2\sin\theta} \quad (3)$$

Where  $h$ ,  $k$  and  $l$  are the miller indices of the planes and  $\theta$  is the Bragg angle (expressed in radians). To achieve the true value of the lattice constant, Nelson-Riley method was used. According to this approach, the estimated lattice constants are plotted against the following error function:

$$F(\theta) = \frac{\cos^2\theta}{2} \left( \frac{1}{\sin\theta} + \frac{1}{\theta} \right) \quad (4)$$

Extrapolation to  $F(\theta) = 0$  yields the true lattice constants. Hence, true  $a_{\text{exp}}$  values were obtained for all milling times.

Finally, Field Emission Scanning Electron Microscopy (FESEM) using a LEO Supra 55 microscope was performed on the milled powders to characterize the dispersion of the Mo particles within the  $\text{Al}_2\text{O}_3$  matrix as well as to identify the composite particle size and morphology.

### 3. RESULT AND DISCUSSION

Figure 1. shows X-ray diffraction patterns of powders milled for 1-15 hours. As shown,  $\text{Al}_2\text{O}_3$  and Mo are the main crystalline phases in powders milled at different times. From Figure 1. one can observe that the width of peaks increases with the milling time which is due to the

decrease of crystallite as the milling progresses [10]. Partial amorphization is also observed in powders characterized by increase in background in the area under the main (1 1 0) peaks of Mo [11]. Peaks of Iron can also be observed in the X-ray diffraction patterns of the milled powders. (Figure 1.) It seems the wt. % of Fe after milling is greater than 1%, because of the accuracy of X-ray diffraction method. This is due to the fact that the alumina is a highly hard material compared to the colliding grinding media (stainless steel balls).

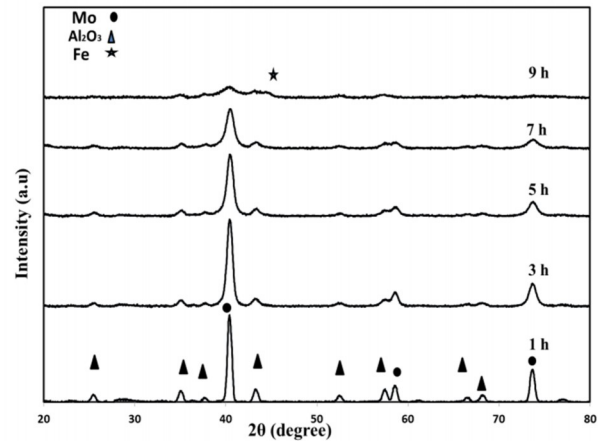
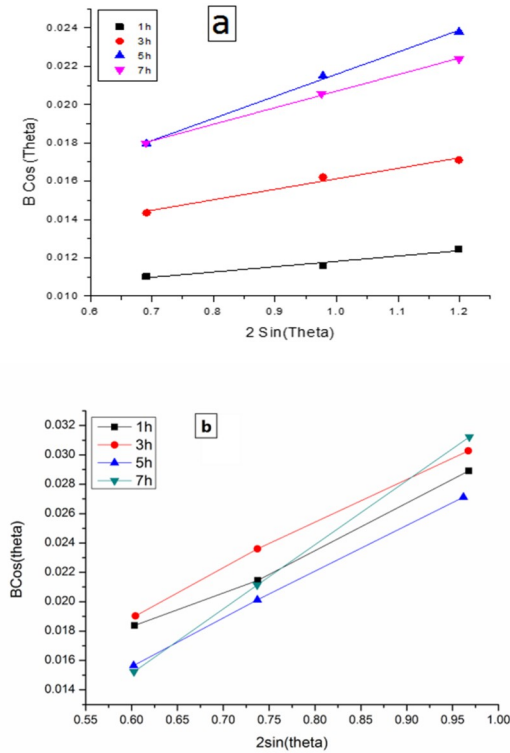


Figure 1. XRD patterns of powders milled.

TABLE 1. Crystallite size and strain as a result of milling for 1-7 h.

	Milling time(h)	Y = a x + b		$d_{\text{Mo}}(\text{nm})$	$\eta_{\text{Mo}}(\%)$	$R^2$
		a	b			
MO	1	0.0028	0.009	15	0.28	0.9619
	3	0.0055	0.0106	13	0.55	0.9838
	5	0.0115	0.01	13	1.12	0.9978
	7	0.0086	0.0121	11	0.86	0.9991
$\text{Al}_2\text{O}_3$	1	0.0293	0.0004	347	2.93	0.9926
	3	0.0308	0.0006	231	3.08	0.9979
	5	0.0318	0.0034	41	3.18	0.9997
	7	0.0437	0.0111	12	4.37	1

Figure 2. presents the plot of “ $B\cos\theta$ ” values versus “ $2\sin\theta$ ” for both Mo and  $\text{Al}_2\text{O}_3$  phases. The results of the linear regression are summarized in Table 1.



**Figure 2.** Crystallite size and strain plots according to the Williamson–Hall method for (a) Mo, and (b)  $\text{Al}_2\text{O}_3$

The plots of the crystallite size and the lattice strain with respect to the milling time are shown in Figure 3. From these plots, it is observed that the crystallite size decreases with the milling time. The work hardening occurs by further increase in milling time and instability increases by crushing of alumina particles and embedding smaller particles into larger ones. Figure 3. also shows that the lattice strain of Mo particles increases by the particle size reduction. This may be explained by increase in the dislocations density as a result of lattice distortion caused by the impact energy of colliding milling balls [12]. However, the lattice strain diminishes quickly as the milling time reaches 5 hours. The reason of drop in the strain may be an offset between the dislocations when the number of defects exceeds the maximum through mechanical milling. Furthermore, milling can cause a temperature rise because of the heat generated by collisions and due to the friction between the milling balls and the particles [13]. Figure 4. shows the plot of the lattice parameter,  $a_{\text{exp}}$ , versus  $F(\theta)$ . The lattice parameters were calculated based on the peak position of each Mo diffraction phase [14]. The estimated true lattice parameters based on the Nelson-Riley method are presented in Table 2. As can be seen from Table 2. the obtained values are very close to the values expected for Mo phases, i.e.  $3.1472\text{\AA}$  [15-17]. According to Table 2. there are some micro-strains in the Mo phases which

may be attributed to the ball-ball and ball-wall heavy impact during the milling process [18]. Figure 5. shows the variations of lattice strain of Mo with milling time.

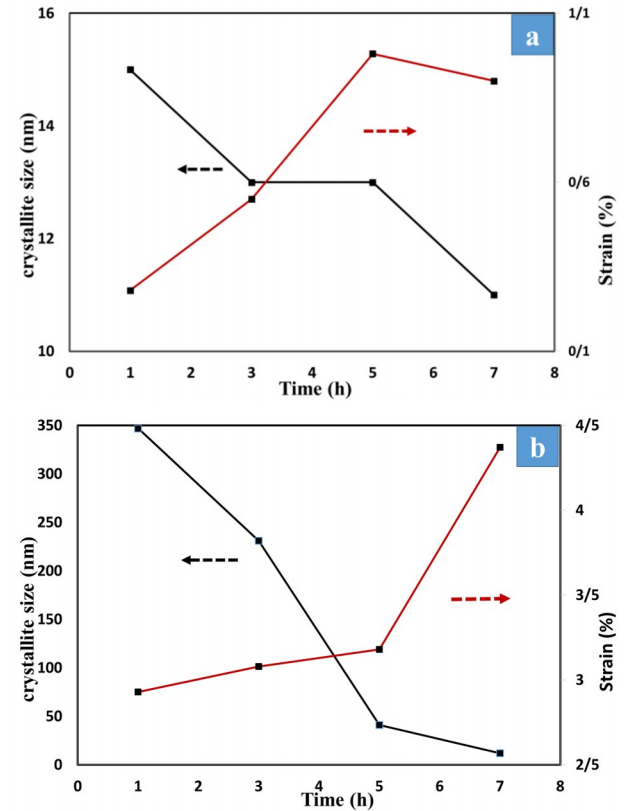


**Figure 3.** Variations of lattice strain and crystallite size with milling time in (a) Mo and (b)  $\text{Al}_2\text{O}_3$ .

**TABLE 2.** Lattice parameter of Mo based on Nelson-Riley method.

Milling time	$(\text{\AA})a_{\text{exp}}$	$(\text{\AA})\Delta\alpha = a_{\text{ST}} - a_{\text{exp}}$
1	3.1454	0.0018
3	3.1447	0.0025
5	3.1444	0.0028
7	3.1432	0.0040

These results indicate that the true lattice parameter decreases as the milling progresses. This phenomenon may be explained by following justifications:

- I. The network shrinks by increasing the milling time due to the incorporation of Iron and considering the fact that the ionic radius of Iron ( $1.72\text{\AA}$ ) is lower than that of Mo ( $2.01\text{\AA}$ ).
- II. The formation of defects and the increase in the micro-strain caused by mechanical impacts causes the network to be distorted.

SEM Images of  $\text{Al}_2\text{O}_3$ -20Vol.%Mo mixture powders presented in Figure 6. show the size and the

morphological evolution during the milling. Without any milling (Figure 6a.) the particles are irregular and inhomogeneous in size distributions. It is found that the powder morphologies are significantly varied with respect to the ball milling time. As the ball milling starts, a noticeable increase in the particle size can be observed. This could be attributed to the cold welding in initial stages of the milling among the particles which results in formation of condensations wherein several particles are held together loosely at point contact [19]. As the milling progresses, the particles get work-hardened and a reduction in the particle size is observed as shown in Figure 6c. Particles are regular and fine after 5 hours of milling. After the 5-hour stage, an increase in the particle size can be observed. This may be due to the fact that further milling causes a temperature rise in the particles. Thus, it can be understood that a balance is established between the cold welding and the brittle fracture and a steady state is reached. Particle size becomes stabilized and no change is observed with further milling. When the milling time reaches 9 h, the particle size is maintained at a stable value. A similar trend has been reported by other researchers investigating the effect of milling time on the mechanical alloying of CNTs/Al-2024 composite powders [19].

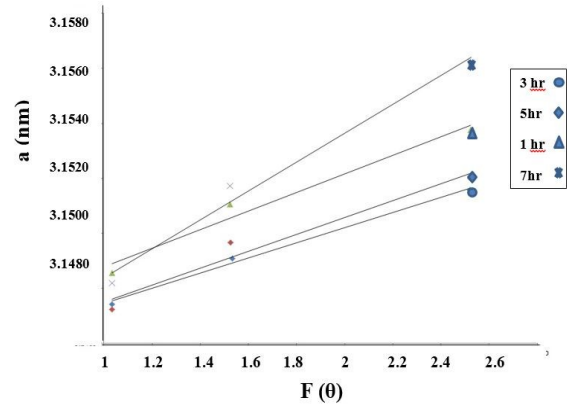


Figure 4. Lattice parameter based on Nelson-Riley analysis.

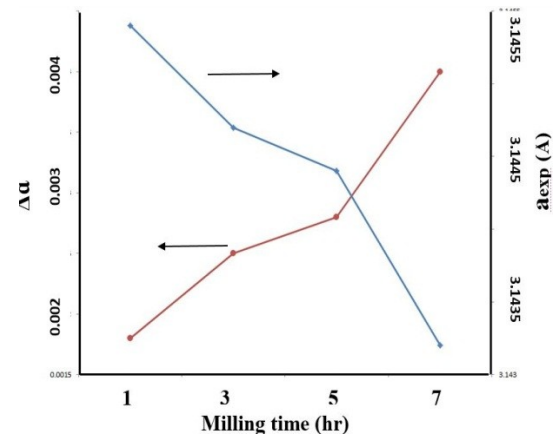


Figure 5. Variations of lattice strain of Mo with milling time.

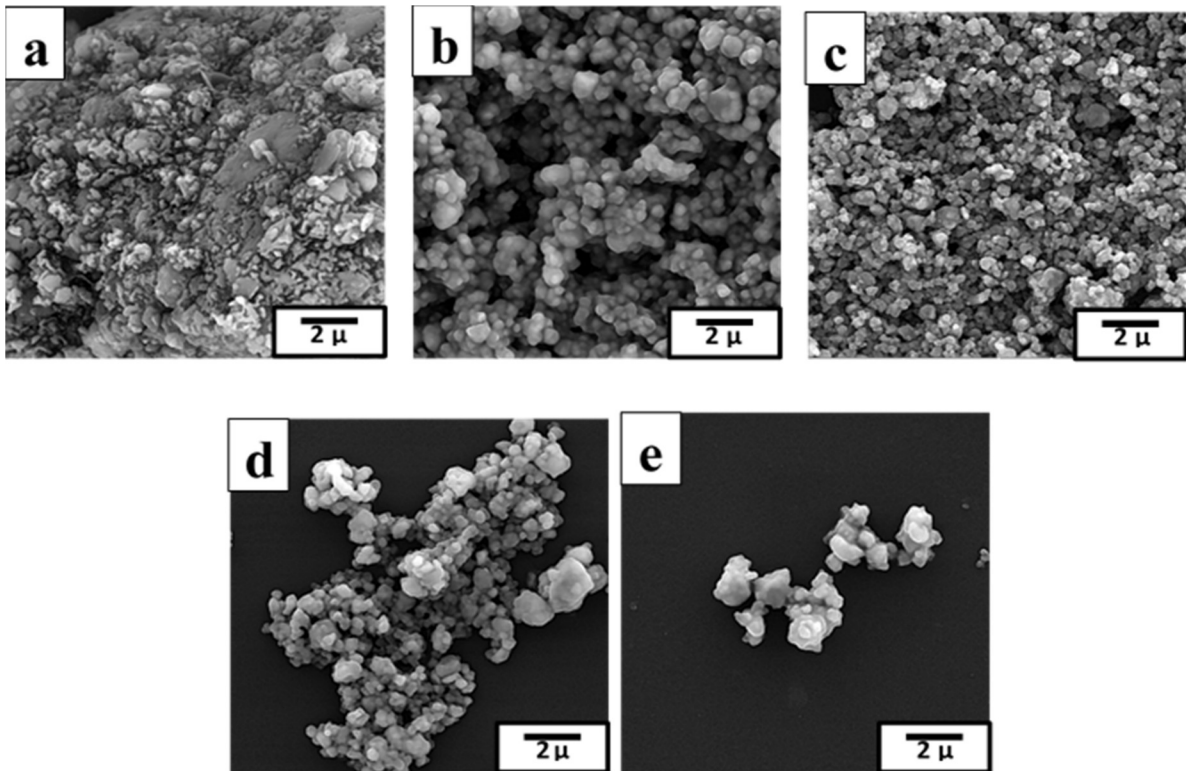
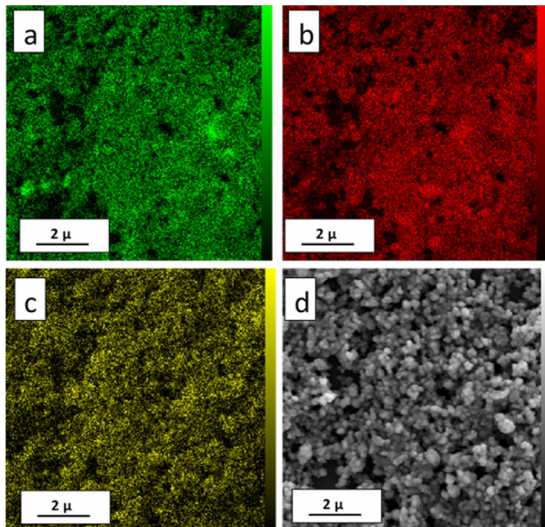


Figure 6. Images (SEM) of Al<sub>2</sub>O<sub>3</sub>-20.Vol% Mo mixture, which was (a) without milling, milled for (b) 3 h, (c) 5 h, (d) 9 h and (e) 15 h.

The SEM elements maps for the milled powders after 5 hours of milling are shown in Figure 7. These images confirm the presence of fine particles and a homogenized mixture between the Molybdenum and the alumina particles while the particles being distinctly differentiated.



**Figure 7.** SEM elements map for 20Mo-80Al<sub>2</sub>O<sub>3</sub> (vol. %) milled for 5 h at x10000 magnification (a) Mo, (b) Al, (c) O and (d) surface.

#### 4. CONCLUSION

1. Al<sub>2</sub>O<sub>3</sub>-Mo nanocomposite was produced successfully after milling for 5 h.
2. The volume of the unit cell was decreased by introducing Iron in the unit cell of the milled powders.
3. Crystallite sizes of alumina-molybdenum powders were in nano-meter scale. Furthermore, the crystallite size and the mean strain decreased as the milling time increased.
4. Microstructural studies using SEM imaging showed that molybdenum particles were homogeneously distributed as the second phase in the alumina matrix.

#### 5. ACKNOWLEDGMENTS

This work was supported by the Materials and Energy Research Center.

#### REFERENCES

1. Khan, H.R. and Siddiqui, M.A., "Effect of Milling Time on Al-Fe-Cr-20 Wt. % Al<sub>2</sub>O<sub>3</sub> composite Prepared Through Ball Milling", *Engineering Research and Applications*, Vol. 4, No. 7, (2014), 183-187.
2. Ramezani, M. and Neitzert, T., "Mechanical milling of aluminum powder using planetary ball milling process", *Journal of Achievements in Materials and Manufacturing Engineering*, Vol. 55, No. 2, (2012), 790-798.
3. Suryanarayana, C., "Mechanical alloying and milling", *Progress in Materials Science*, Vol. 46, No. 1, (2001), 1-184.
4. Zuhailawati, H. and Jamaludin, S., "Studies on mechanical alloying of Copper-Tungsten Carbide composite for spot welding electrode", *Journal of Materials Engineering and Performance*, Vol. 18, No. 9, (2009), 1258-1263.
5. Nawa, M., Sekino, T., and Niihara, K., "Fabrication and mechanical behaviour of Al<sub>2</sub>O<sub>3</sub>/Mo nanocomposites", *Journal of Materials Science*, Vol. 29, No. 12, (1994), 3185-3192.
6. Sekino, T. and Niihara, K., "Microstructural characteristics and mechanical properties for Al<sub>2</sub>O<sub>3</sub>/metal nanocomposites", *Nanostructured Materials*, Vol. 6, No. 5, (1995), 663-666.
7. Chmielewski, M., Dutkiewicz, J., Kaliński, D., Lityńska, L., Pietrzak, K. and Strojny-Nędza, A., "Microstructure and properties of hot-pressed molybdenum-alumina composites", *Archives of Metallurgy and Materials*, Vol. 57, No. 3, (2012), 687-693.
8. Weglewski, W., Basista, M., Chmielewski, M. and Pietrzak, K., "Modeling of thermally induced damage in the processing of Cr-Al<sub>2</sub>O<sub>3</sub> composites", *Composites Part B: Engineering*, Vol. 43, No. 2, (2012), 255-264.
9. Sbaizero, O. and Pezzotti, G., "Influence of the metal particle size on toughness of Al<sub>2</sub>O<sub>3</sub>/Mo composite", *Acta Materialia*, Vol. 48, No. 4, (2000), 985-992.
10. Kumari, S., Singh, D.K. and Giri, P., "Strain anisotropy in freestanding germanium nanoparticles synthesized by ball milling", *Journal of Nanoscience and Nanotechnology*, Vol. 9, No. 9, (2009), 5231-5236.
11. Wu, W.-W., Zhang, G.-J. and Sakka, Y., "Nanocrystalline ZrB<sub>2</sub> powders prepared by mechanical alloying", *Journal of Asian Ceramic Societies*, Vol. 1, No. 3, (2013), 304-307.
12. Khan, H.R. and Siddiqui, M.A., "Characterization of Al-Fe-Cr-Al<sub>2</sub>O<sub>3</sub> composites with varying weight percentage of alumina fabricated through mechanical alloying", *International Journal of Applied Science and Engineering Research*, Vol. 3, No. 4, (2014), 782-791.
13. Zhang, F., Lu, L., Lai, F., M.O. and Froes, F.H., "Grain growth and recrystallization of nanocrystalline Al<sub>3</sub>Ti prepared by mechanical alloying", *Journal of Materials Science*, Vol. 38, No. 3, (2003), 613-619.
14. De Souza, R.F.B., Parreira, L.S., Rascio, D.C., Martins Silva, J.C., Neto, E.T., Calegari, M., V. Spinacé, E., Neto, A.O. and Santos, M.C., "Study of ethanol electro-oxidation in acid environment on Pt<sub>3</sub>Sn/C anode catalysts prepared by a modified polymeric precursor method under controlled synthesis conditions", *Journal of Power Sources*, Vol. 195, No. 6, (2010), 1589-1593.
15. Klug, H.P. and Alexander, L.E., "X-ray diffraction procedures", (1954).
16. Nelson, J.B. and Riley, D., "An experimental investigation of extrapolation methods in the derivation of accurate unit-cell dimensions of crystals", *Proceedings of the Physical Society*, Vol. 57, No. 3, (1945), 160-177.
17. Razavi, M., Rahimpour, M. and Yazdani-Rad, R. "Synthesis of Fe-WC nanocomposite from industrial ferrotungsten via mechanical alloying method", *Advances in Applied Ceramics*, Vol. 110, No. 6, (2011), 367-374.
18. Zakeri, M., Zanganeh, T. and Najafi, A., "High-frequency induction heated sintering of ball milled Fe-WC nanocomposites", *International Journal of Minerals, Metallurgy, and Materials*, Vol. 20, No. 7, (2013), 693-699.
19. Hao, X.-n., et al., "Effect of mechanical alloying time and rotation speed on evolution of CNTs/Al-2024 composite powders", *Transactions of Nonferrous Metals Society of China*, Vol. 24, No. 7, (2014), 2380-2386.